HHS Public Access

Author manuscript

Adv Healthc Mater. Author manuscript; available in PMC 2017 July 01.

Published in final edited form as:

Adv Healthc Mater. 2016 July ; 5(14): 1800–1807. doi:10.1002/adhm.201500936.

Human skin constructs with spatially-controlled vasculature using primary and iPSC-derived endothelial cells

Hasan E. Abaci[1], **Zongyou Guo**[1], **Abigail Coffman**[1], **Brian Gillette**[2], **Wen-han Lee**[2], **Samuel K. Sia**[2], and **Angela M. Christiano**[*,1,3]

[1]Department of Dermatology, Columbia University Medical Center, New York

[2]Department of Biomedical Engineering, Columbia University, New York

[3]Department of Genetics and Development, Columbia University Medical Center, New York

Abstract

Vascularization of engineered human skin constructs is crucial for recapitulation of systemic drug delivery and for their long-term survival, functionality, and viable engraftment. In this study, we used the latest microfabrication techniques and established a novel bioengineering approach to micropattern spatially-controlled and perfusable vascular networks in 3D human skin equivalents using both primary and induced pluripotent stem cell (iPSC)-derived endothelial cells (ECs). Using 3D printing technology, we were able to control the geometry of the micropatterned vascular networks. We verified that vascularized human skin equivalents (vHSEs) can form a robust epidermis and establish an endothelial barrier function, which allows for the recapitulation of both topical and systemic delivery of drugs. In addition, we examined the therapeutic potential of vHSEs for cutaneous wounds on immunodeficient mice and demonstrated that vHSEs can both promote and guide neovascularization during wound healing. Overall, this innovative bioengineering approach could enable *in vitro* evaluation of topical and systemic drug delivery, as well as improve the potential of engineered skin constructs to be used as a potential therapeutic option for the treatment of cutaneous wounds.

Keywords

Engineered skin; vasculature; microfluidics; patterning; iPSC

[*] amc65@cumc.columbia.edu.

Author contributions: H.E.A. designed the microfabrication experiments, performed majority of the experiments, analyzed the data and wrote the manuscript. Z.G. performed differentiation experiments and reviewed the manuscript. A.C. performed microfabrication experiments, did quantifications and reviewed the manuscript. B.G. designed the microfabrication experiments. W.L. performed CAD drawings and design modifications. S.K.S. designed the microfabrication experiments and reviewed the manuscript. A.M.C. designed the study, discussed the data, and wrote and reviewed the manuscript.

Supporting Information

Supporting Information is available from the Wiley Online Library or from the author.

Competing interests: The authors declare no conflict of interest.

1. Introduction

The ability to generate engineered human skin constructs has provided a valuable *in vitro* platform to evaluate drug candidates and a promising therapy for acute or non-healing large cutaneous wounds that affect millions of patients each year. Commercially available skin constructs are typically composed of only keratinocytes and fibroblasts, and have limitations including poor viability and integration, essentially leading to formation of a non-functional scarred skin [1, 2].

In order for a skin graft to integrate effectively, it must attach well to the wound bed, avoid rejection by the immune system, and most importantly, be supported by new vasculature. Vascularization is required for proper and long-lasting structure and function of 3D skin constructs. Perfusion of the dermal component by vascular structures allows for rapid and efficient exchange of oxygen and nutrients, which ensures rapid take and long-term survival of skin grafts [3]. Thus, the availability of an engineered skin construct with a functional vasculature could address the aforementioned clinical challenges to treat cutaneous wounds.

Recently, incorporation of induced pluripotent stem cell (iPSC)-derived skin cells into skin constructs has shown promise in achieving a sufficient number of skin cells and reduction in the rate of rejection by the immune system [4]. Similarly, bioengineering full thickness skin constructs containing lymph and blood capillaries represented an important step towards preventing graft necrosis[1, 5-7]. Moreover, with the recent availability of endothelial cell (EC) differentiation protocols, it has become possible to use iPSC-derived ECs in hydrogel scaffolds to promote wound healing [8]. In these studies, endothelial cells were encapsulated as single cells in hydrogels and stimulated to spontaneously form capillary-like structures that are typically randomly distributed or poorly organized. Formation of organized vascular structures prior to engraftment, on the other hand, may improve the success of integration into host vasculature and survival of engrafted tissue, as previously shown for muscle tissue [9]. In addition, when capillary-like structures are formed in physiological scaffolds, such as collagen or fibronectin, they tend to regress, as rapidly as 24 hours [10]. Recently, several engineering techniques have been developed to create interconnected *in vitro* vascular networks in hydrogels [11-16]. However, adapting these techniques to micropattern vascular structures in 3D skin constructs that are prepared using physiological biomaterials is particularly challenging due to high contractile nature of dermal fibroblasts in soft 3D gels, such as uncrosslinked collagen [17].

Current efforts focused on sytemic delivery of drugs to/from skin rely on animal models, which fail to truly represent human physiology. Despite the potential of engineered 3D human skin constructs for drug discovery, it is only limited to evaluation of topical drug delivery due to lack of a perfusable vasculature. Therefore, an *in vitro* platform that can effectively recapitulate cutaneous microcirculation has been a prevailing need for such studies. Although several vascularized skin constructs have been previously developed [1, 5-7], they did not allow for *in vitro* perfusion of skin vasculature or evaluation of endothelial barrier function.

In this paper, we developed a novel strategy to bioengineer human skin equivalents (HSEs) with perfusable and pre-organized vasculature using both primary and iPSC-derived ECs. Our study, to our knowledge, represents the first *in vitro* skin model (i) with an embedded perfusable vasculature that allows for the study of systemic delivery of therapeutics and (ii) with an iPSC-derived vasculature. We also demonstrate that these vascularized HSEs (vHSEs) can promote and guide neovascularization during wound healing in mice. Thus, in addition to serving as an *in vitro* drug screening platform, the vHSEs may also contribute to a better engraftment, long-term survival and enhance functionality of skin substitutes, which remains an unmet medical need for many regenerative medicine applications.

2. Results

2.1. Micropatterning vascular networks in human skin equivalents

We established a novel method to incorporate perfusable 3D vascular networks into HSEs using type I collagen, which is the most abundant ECM protein in the skin and is found in its natural uncross-linked state. We utilized 3D printing technology to build molds for desired vasculature patterns, inlet/outlet tubes for perfusion and ring-shaped holders to precisely position the vascular networks in the HSEs (**Figure 1A** and **Figure S1A**). The 3D-printed molds were used to make sacrificial microchannels of cross-linked alginate which were later embedded in the dermal compartment that is composed of collagen gel (2.7 mg/ml) and human dermal fibroblasts. Alginate molds with a diameter of 400 μm yielded sacrificial microchannels with an average diameter of 300 μm. Subsequently, epidermalization was achieved by plating the keratinocytes on top of the dermal compartment, followed by bringing the HSE to an air-liquid interface for cornification, as previously described [18, 19]. We used a physillogically-relevant ECM, uncrosslinked type I collagen gel, which typically undergoes a significant contraction during skin reconstruction, especially after the addition of keratinocytes [20]. During the epidermalization step in our experiments, we observed ~ 15 fold and 2 fold reduction in thickness and diameter, respectively, where collagen gel remained attached on the membrane (**Figure S1B**). This significant contraction of the 3D skin constructs introduced an engineering design challenge once we incorporated the perfusable microchannels into the system. The 3D-printed ring-shaped holders allowed us to precisely position the sacrificial channels in collagen gel with an offset of 1 mm from the membrane surface, achieving a closed system despite the substantial contraction. Dissolving and removing the alginate microchannels by perfusing a sodium citrate solution (5%) through the inlet tubes formed open channels that allow for continuous perfusion of media or cell-suspension using an external pump (**Figure S1C**). After the channels were dissolved in HSEs, their original diameter decreased, varying in a range of 100-250 μm, due to further contraction of the collagen gel. This size was significantly larger than the capillaries (<50 μm) and slightly larger than the size of the arterioles (<100 μm) in the human skin[21]. Nevertheless, using our method, we were able to make smaller channels (<100 μm) to mimic relatively small capillaries (**Figure S1D**). For the rest of the study, we chose to use channels >100 μm, since they allowed for a lower pressure drop, and thus a continuous perfusion without causing significant leakage.

Perfusion of these channels with a suspension of GFP-tagged HUVECs demonstrated the pre-organized vascular formation in HSEs (**Figure S2A**) where the vasculature was surrounded with dermal fibroblasts as shown by reconstructed confocal images of vHSEs immunolabeled with vimentin (**Figure S2B**). We observed that when the sacrificial layer was dissolved before the skin constructs were fully contracted, remodeled and cornified, the channels tended to close, collapse or merge. Thus, the timing of sodium citrate treatment was critical to maintain the size and pattern of the vascular networks.

This new bioengineering approach allowed us to micropattern different designs of microchannel networks in HSEs. For this study, we used two different patterns: i) a simple pattern composed of two channels; and ii) a more physiologically relevant pattern mimicking vascular bifurcations and providing a better coverage of the skin construct surface area for uniform exchange of nutrients (**Figure 1B**).

2.2. Vascularized HSEs form epidermal layers and endothelial barrier function

We examined the formation of epidermal layers and the endothelial barrier function in vHSEs constructed using both GFP-tagged HUVECs and iPSC-derived ECs (iECs) (**Figure S3**). Immunolabeling and Hematoxylin and Eosin (H&E) staining of the histological sections of vHSEs containing the physiological vascular pattern showed the presence of the hollow microchannels and coating of the inner walls of these channels with HUVECs (**Figure S4**) and iECs (**Figure 2Ai**). Immunostaining of the vHSE sections with a differentiation marker K10, a basal layer marker, K14, and a corneum specific marker, loricrin showed that all of the epidermal layers were established (**Figure 2Aii**).

To test the endothelial barrier function of vHSEs, we performed diffusion experiments by perfusing a FITC-dextran (70kDa) solution through the microchannels covered with HUVECs and iECs in comparison to the microchannels containing dermal fibroblasts or no cells. For these experiments, we used the simple pattern, which is composed of two parallel channels with a uniform non-vascular region in between, allowing for reliable quantification of the diffusion. We measured the diffusion rate of the dye solution into the collagen gel by detecting the changes in fluorescence intensity over time. Subsequently, by performing numerical simulations using COMSOL Multiphysics software, we estimated the diffusivity and vascular permeability in vHSEs as a measure of endothelial barrier function (**Figure 2B** and **Figure S5**). HUVECs and iECs exhibited a similar permeability of 0.045 and 0.018 μm/sec, respectively (**Figure 2C**).

These values were significantly lower than the values obtained with control experiments using dermal fibroblast, 1.6 μm/sec, indicating the formation of the endothelial barrier function. The permeability of HUVECs and iECs to 70 kDa Dextran was found to be similar but slightly lower than the previously reported values of 0.05-0.15 μm/sec [22] and 0.06 μm/sec [23] using HUVECs. Due to the limitations of non-invasive imaging techniques, we compared our results with the permeability of rodent microvessels to 70 kDa dextran[24-26]. The permeability values reported by Corovic et. al[24] for mouse cutaneous microvessels (0.008 μm/sec) were approximately 2.5 times lower than of the *v*HSEs. Another recent study[26] using multi-photon microscopy to estimate the permeability of microvessels in mice skin, reported that approximately 90% of the injected 70 kDa dextran molecules

remained in the microvessels after 60 mins, similar to values we showed in Figure 2C for vHSEs (~90% for HUVECs and ~95% for iECs). Moreover, our values more closely mimicked those reported for isolated mammalian venules[25] (approximately 0.02 μm/sec for FITC-albumin [66.5 kDa]). Overall, we demonstrated that vHSEs can form all epidermal layers properly and establish an endothelial barrier function, which allows for recapitulating systemic delivery or removal of drugs.

2.3. Micropatterned vHSEs promote and guide neovascularization during wound healing

We examined the therapeutic potential of vHSEs for cutaneous wounds by grafting onto immunodeficient mice. The vHSEs with HUVECs or iECs were grafted on the back of SCID mice and removed after 5 days or 14 days for the evaluation of graft integration. There was no significant vessel ingrowth in all conditions after 5 days (data not shown). After day 14, vHSEs with HUVECs or iECs were dramatically perfused with blood whereas control HSEs without microchannels (“Control I“) or with acellular microchannels (“Control II“) both remained non-perfused (**Figure 3Ai**). This observation was supported by immunolabeling the histological sections with CD31 antibody specific to mouse endothelial cells (**Figure 3Aii**). We verified that the percentage of the area occupied by the host vasculature in vHSEs were dramatically higher than that in control HSEs, suggesting that vHSEs promote host neovascularization in the grafts (**Figure 3Aiii**). In addition, quantification of Ki-67 immunostained sections (**Figure 3Aii**) demonstrated that the ratio of the proliferating cells to total number of cells was significantly higher in vHSEs than control HSEs (**Figure 3Aii**). More profoundly, 40% of the cells in the basal epidermis layer in vHSEs were proliferative compared to 5% in control HSEs, suggesting that the improved vascularization in vHSEs led to a better maintenance of the proliferative capacity of the basal keratinocytes (**Figure 3Aiii**).

Interestingly, the newly formed host vessels were perfectly aligned with the vasculature pattern in HSEs (**Figure 3Bi**). Perfusion of the host vessels with fluorescently-tagged dextran also indicated that the micropatterned vasculature in vHSEs guides the neovascularization (**Figure 3Bii**). To examine whether such guidance occurred due to the existence of hollow microchannels or signaling from organized human ECs, we performed the same experiment with HSEs which have microchannels but no cells and found that human ECs are required to recruit newly formed vessels (**Figure 3Ai**). Overall, our analyses showed that micropatterned vasculature in vHSEs can both promote and guide neovascularization during graft integration onto the wound, which may potentially lead to improved engraftment of engineered skin constructs.

3. Discussion

Developing a truly functional human skin construct is a major challenge for skin tissue engineering and regenerative medicine. Previous attempts at incorporating different components into skin constructs, to date, have been made by simply mixing the cell type of interest with dermal or epidermal cells at predetermined ratios, followed by stimulating the cells to spontaneously form randomly distributed structures. However, the ability to develop a complex skin construct with multiple components relies on precise control over density,

structure, and arrangement of such components in a 3D microenvironment. To our knowledge, our study represents for the first time: i) the generation of iPSC-derived vasculature in engineered skin grafts; ii) the implementation of the latest 3D-vascularization techniques to create a complex skin tissue with a micropatterned vasculature; and iii) an *in vitro* skin model with an embedded perfusable vasculature that allows for the study of systemic delivery of drugs, which has been a prevailing need for *in vitro* drug screening studies.

Skin constructs in different settings, such as epidermal (only keratinocytes) or full-thickness (keratinocytes and fibroblasts), are broadly being used in pharmaceutical and cosmetic industry to evaluate the toxicity and efficacy of drug candidates [27]. In addition, incorporating different skin components, such as macrophages [28], melanocytes[29] and sweat glands [30], into engineered skin constructs has enabled the development of more reliable human skin models for *in vitro* drug testing studies. Although the topical delivery of drugs can be studied by these models in static culture medium, the systemic delivery of substances to/from skin cannot be effectively recapitulated due to the lack of an endothelial barrier. To address this, microfluidic skin culture platforms have been developed to mimic physiologically relevant blood flow [19, 31]. In such platforms, however, the dermal compartment of skin is not in direct contact with the vasculature and is usually separated from the vasculature by a permeable membrane, which introduces an additional and nonphysiological diffusion barrier. Vascularized skin constructs have been developed previously by several groups [1, 5-7], although they did not allow for the evaluation of the endothelial barrier function simply because the vasculature in those studies was spontaneously formed and thus not perfusable. Moreover, our vHSEs with a perfusable vasculature showed improved endothelial barrier function (0.045 and 0.018 μm/sec for HUVECs and iECs) compared to previous *in vitro* studies (0.05-0.15 μm/sec[22, 23]), focused on developing 3D microvessels in hydrogels (but not in skin constructs), and served as a closer mimic of the physiological values reported for cutaneous vessels in mice (0.008 μm/sec) [24]. This improvement may be due to the presence of dermal fibroblasts and keratinocytes, which significantly remodel the collagen matrix during epidermilization process [32, 33].

In our *in vivo* functionality experiments, we showed that pre-organized vasculature in vHSEs can promote the host neovascularization and induce vessel invasion from the wound bed towards the epidermis. Similarly, others previously showed an improved graft integration using skin constructs with spontenously formed cappilaries [5, 6]. On the other hand, Koffler et al. previously showed that[9] engineered skeletal muscle grafts having pre-organized vasculature, as opposed to spontaneously formed capillaries, enhanced the neovascularizton in the grafted tissue. Therefore, using HSEs with pre-organized vasculature may be an advantageous strategy over previous approaches in terms of graft integration. However, we were not able to make a direct comparison between the vHSEs and spontaneously formed capillaries in HSEs, due to the fact that spontaneously formed capillary structures in collagen gels tend to regress as early as 24 hours, as previously demonstrated [10]. Interestingly, we found that the newly formed mice vessels were aligned with the micropatterns in vHSEs. This has been shown previously for other cell types, such as neurons[34], that microchannels can promote the migration and guide the regeneration of

tissues. However, whether the neovascularization can potentially be directed by controlling 3D-printed vasculature patterns requires further investigation.

We recently developed skin constructs using iPSC-derived fibroblasts, keratinocytes and/or melanocytes [4, 29, 35, 36]. Here, we successfully incorporate iPSC-derived ECs into skin constructs. Using iPSC-derived ECs can be highly beneficial for developing vascular - related disease models such as diabetes and psoriasis as well as potentially addressing the current issues of immune rejection of skin grafts using patient specific iPSC-derived cells. Although our vHSEs can potentially allow for long-term graft survival, it will be necessary to include multiple skin components alongside vasculature to bioengineer a truly functional skin construct with a sufficient level of complexity. For example, the addition of hair follicles, which are highly vascularized, into HSEs still remains a challenge for tissue engineering and regenerative medicine [37]. The utilization of engineered skin constructs as a potential therapeutic option for cutaneous wounds will undoubtedly require developing more physiologically relevant skin constructs. The ability to spatially control the vascular formation in HSEs will greatly help achieve this goal by effectively meeting the metabolic demand of the skin components.

4. Experimental Section

Cell Culture

Neonatal dermal fibroblasts and keratinocytes were isolated from human foreskin and cultured in DMEM with 10% FBS and in CnT-07 (Zenbio), respectively. GFP-tagged HUVECs (Angio-proteomie) were cultured in tissue culture plates coated with a quick coating solution (Angio-proteomie) and maintained in endothelial cell growth medium (Angio-proteomie). Culture medium was changed every other day for all cell types. The cells were kept in a humidified incubator at 37 °C and 5% CO_2.

Generation of iPSCs and EC Differentiation

Integration-free iPSCs were established as previously described [38, 39]. Briefly, human fibroblasts from foreskin were electroporated with episomal vectors containing OCT3/4, SOX2, KLF4 and L-Myc. 7 days after transfection, cells were trypsinized, plated on Mitomycin C (MMC)-treated mouse embryo fibroblast (MEF) feeder layer and maintained in iPSC medium (KO DMEM supplemented with 20% KO serum replacement, 1% GlutaMAX-I, 1% nonessential amino acid, 1% penicillin-streptomycin, and 4 ng/ml basic FGF). 3-4 weeks after transfection, colonies with a flat human embryonic stem cell (ESC)-like morphology emerged, and were manually picked up for expansion and for validation of stem cell markers and the pluripotency [4].

Endothelial cells were differentiated from iPSCs by using small molecules to activate the WNT pathways [40]. In brief, iPSCs were dissociated into single cells and plated onto Matrigel-coated dishes in mTeSR1. After treatment with 8 μM CHIR99021 for 2 days in Advanced DMEM/F12 containing 60 μg/ml ascorbic acid, cells were expanded in EGM-2 for characterization. The iECs have been characterized in terms of their expression of CD31 (1:50, Abcam), VECAD (1:200, Fisher Scientific) (**Figure S3**). In addition, LDL-uptake

assay was conducted by incubation with 8ng/mL Alexa Fluor 594 acetylated low-density lipoprotein (cat. # L35353; Invitrogen) for 4h. After rinsing with PBS, the cells were photographed with a fluorescence microscope. The ability of iECs to form tube-like structures was tested by seeding 200,000 cells per well of 12-well plates coated with 100 μl/well of growth factor-reduced Matrigel-coated plates in EGM-2 medium supplemented with 50 ng/ml vascular endothelial growth factor (VEGF) overnight.

Micropatterning Vasculature in Skin Constructs

All 3D-printed tools were designed and drawn using the computer-aided design (CAD) software, Solidworks Student Edition 2015. Molds for casting alginate sacrificial channels with 400 μm in width and depth were 3D-printed using Objet24 3D-Printer (Stratasys) which uses a UV-curing material, VeroWhite (Stratasys). Similarly, inlet and outlet inserts as well as ring-shape holders were 3D-printed, connected to each other and placed on the channel molds (**Figure S1A**). Alginate solution (5% w/w in dH_2O) was sterilized using syringe filters, pipetted onto the channel molds and soaked in 10% w/w calcium chloride solution for crosslinking for 15 mins. Then the crosslinked alginate channels attached to the ring-holder and inserts were removed from the mold and kept on a heating plate at 60 °C until the channels were completely dried, making the alginate attach to the inserts more strongly and the system easier to handle. 3D-printed molds with a diameter of 400 μm yielded sacrificial microchannels with an average diameter of 300 μm. After the channels are dissolved in HSEs, this diameter decreases and varies in a range of 100-250 μm, due to contraction of the collagen gel.

Sacrificial alginate channels were suspended in transwell inserts (polyethylene terephthalate membranes, 3 μm pore size, Corning) placed in a 6 deep well plate (Corning) (**Figure 1A**). 3D skin equivalents were generated in these transwell inserts similar to the method described previously (all media formulations can be found in refs [[18] and [36]]). The dermal compartment was prepared by adding 4 ml of type I collagen matrix containing 1.25×10^5 fibroblasts/ml into the transwell inserts and polymerized around the sacrificial alginate channels. After polymerized matrix was cultured for 7 days, 1×10^6 keratinocytes were plated on the matrix and the construct was cultured submerged within epidermalization medium[18] for additional 7 days. Subsequently, the constructs were cultured in cornification medium[18] and maintained at an air-liquid interface for 7 days. After the cornification is complete, the chamber was washed with PBS, and the constructs were treated with sodium citrate solution (5% w/w in PBS) for 15 mins at the air-liquid interface at 37 °C to dissolve the sacrificial channels. Then sodium citrate solution was injected through the inlet insert to remove the remaining alginate, forming hollow channels. The sodium citrate solution in the channels was then washed out by injecting PBS and DMEM+10%FBS. There was no significant toxic effect of sodium citrate on the epidermalization process, due to low exposure time and optimized concentration. After a recovery period of 12 hours in cornification medium, HUVECs or iECs were resuspended in the endothelial growth medium- 2 (EGM-2, Lonza) at a cell density of 6 million cells/ml and seeded by injecting 200 μl of cell suspension. Constructs were cultured in a mixture of cornification and EGM-2 media (1:3 ratio) at the air-liquid interface for 2 days. Subsequently, the skin constructs were either used for *in vitro* perfusion experiments or grafted onto mice.

Estimation of Endothelial Barrier Function

Skin constructs containing microchannels with or without fibroblasts, HUVECs or iECs (N=3) were perfused with a 70 kDa FITC-dextran solution (10 μmol/L) and imaged every 5 mins using Olympus SZX16 microscope for 60 mins. The samples were imaged every 5 mins at an exposure time of 0.5 seconds and were not illuminated in between captures, yielding a total actual exposure time of 6 seconds throughout the experiment. To take into account the effect of photobleaching, we performed control experiments only with FITC-dextran and found <5% decrease in the fluorescence after 1 hour. ImageJ software was used to detect the fluorescent intensity at 3 points along the width of each channel as well as 3 points outside the channels along the horizontal centerline of the vascular pattern. The data was then used to estimate the endothelial permeability by performing implicit time-dependent simulations, using the “diffusion module”, based on finite element methods with an extremely fine meshing size and a relative tolerance of 0.01 min using COMSOL Multiphysics software v4.4. Simulations were run by changing the diffusivity values to give the best fit to the experimental data using the least sum of squares method. First, the data for acellular microchannels was used to estimate the diffusivity of 70 kDa dextran in skin construct matrix. Then, this value was plugged into the simulations to estimate the permeability of microchannels containing fibroblasts, HUVECs and iECs.

Immunostaining and Imaging

For immunostaining analyses, samples were either embedded in paraffin wax or cryopreserved in OCT solution. Formalin (10%) fixed, paraffin wax embedded tissues were cut (15 μm) onto poly-L-lysine-coated slides, dried overnight at 55°C, dewaxed in xylene and rehydrated through a graduated ethanol series (100%, 95%, 70%) and distilled water (dH2O). Antigen retrieval was performed by incubating at 95 °C as previously described [19]. Samples were rinsed briefly with PBS and blocked using 2% fish skin gelatin (Sigma) in PBS containing 0.025% Triton-X-100 for 90 minutes at RT. Samples were incubated with primary antibodies (Keratin 1, 1:1000, Covance, Keratin-14, 1:1000, Covance, Loricrin, 1:500, Covance, Ki67, 1:1000 BD Biosciences, CD31, 1:50, Abcam and human-specific CD31, 1:200, R&D Systems) overnight at 4°C. After washing with PBS, samples were incubated with fluorophore-conjugated secondary antibodies (Donkey anti-Rabbit 594, and Goat anti-mouse 488, 1:700, Invitrogen) for 2 hours at RT. Slides were covered with cover-slips using mounting medium containing 4’,6-diamidino-2-phenylindole (DAPI) (Vectashield) and examined using a Zeiss LSM 5 Exciter confocal laser scanning microscope.

Image Analyses and Quantification

The degree of vascularization and proliferation were evaluated based on the quantification of the total surface area covered by CD31 positive cells and the ratio of Ki67 positive cells, respectively. Quantification was performed using the cell analyses software CellProfiler as previously described [41]. Images taken from six different regions in each sample (N=4 for all conditions) were used for all analyses. For vascularization, the total area that was positive for CD31 expression was identified by the software. The vascular occupation was calculated by the ratio of this area to the total area in each image. The dermis and basal layer were

manually selected on each image as the region of interest. For each region, Ki67-positive cells and cell nuclei were identified and counted. The ratio of the Ki67-postive cells to total number of cells was used to evaluate the proliferation of the cells in dermis and keratinocytes in the basal layer separately.

Haematoxylin and Eosin Staining (H&E)

Dewaxed 15 μm sections were stained with Mayers Haematoxylin (Sigma) at RT for 3 minutes. Blue staining was performed by rinsing in tap water while differentiation was achieved by rinsing in 1% acid ethanol. Counterstaining was performed by rinsing with eosin (Sigma) for 30 seconds and dehydration was performed by sequential washing with 95% ethanol, 100% ethanol and Histo-Clear (National Diagnostics). Slides were covered with cover-slips with DPX (Agar Scientific) and examined by light microscopy using a Zeiss Axioplan 2 microscope.

Engraftment on Mice

All experimental animal protocols were approved by the Institutional Animal Care and Use Committee at Columbia University Medical Center. 0.8 cm of skin was removed from the dorsal antero-posterior midline surface of 8–10 week old SCID mice (Charles River, Wilmington, MA) using the pinch cutting technique (**Figure S6i**). The vHSEs were placed on the recipient and secured with 4 sutures (7-0 Nylon) in a simple interrupted pattern around the edge of the graft (**Figure S6ii**). To protect the equivalent, we used a method described for the establishment of a humanized skin model [42], whereby the skin removed from the mouse was freeze-thawed 3 times by placing in DMEM, then inserting into liquid nitrogen prior to warming in a beaker of water. This decellularized and devitalized the skin, which was placed back over the skin construct on the mouse. The decellularized skin was sutured in place with interrupted sutures (**Figure S6iii**). A Bandaid was then wrapped around the mice (an OpSite Flexifix Transparent Film) to hold the graft in place. The mice were euthanized after 5 days or 2 weeks for analyses. The mice were injected intravenously through tail vein with Rhodamine-dextran (10 mg/ml) solution 20 min prior to euthanasia to visualize the vascularization. [9] After 5 days or 14 days (**Figure S6iv**), the constructs were harvested for analyses. Mice experiments were performed at N=4 for all conditions tested.

Statistical Analysis

The statistical analysis was performed using two-tailed paired t-test with 95% confidence interval with the software GraphPad Prism. For testing endothelial barrier function, 3 skin constructs per condition and for *in vivo* testing 4 mice per condition were used. $P < 0.05$ was considered significantly different. Data was shown as means ± SEM.

Supplementary Material

Refer to Web version on PubMed Central for supplementary material.

Acknowledgements

We thank Ming Zhang, Emily Chang and Jade Huang for their expert technical assistance and Dr. Chong Shen for characterization of iPSC-derived ECs. **Funding**: This project was funded by the National Center for Advancing

Translational Sciences at the National Institutes of Health (5U18TR000561-02: Modeling complex diseases using iPSC-derived skin constructs), the National Institute of Arthritis and Musculoskeletal and Skin Diseases (5P30AR044535-14: Columbia University Medical Center Skin Disease Research Center) and New York State Stem Cell Science (IDEA C029550: Skin Cell and iPSC Therapy for Epidermolysis Bullosa).

References

1. Supp DM, Wilson-Landy K, Boyce ST. FASEB journal : official publication of the Federation of American Societies for Experimental Biology. 2002; 16:797. [PubMed: 12039861]
2. Maione AG, Brudno Y, Stojadinovic O, Park LK, Smith A, Tellechea A, Leal EC, Kearney CJ, Veves A, Tomic-Canic M, Mooney DJ, Garlick JA. Tissue engineering. Part C, Methods. 2015; 21:499. [PubMed: 25343343]
3. Bottcher-Haberzeth S, Biedermann T, Reichmann E. Burns : journal of the International Society for Burn Injuries. 2010; 36:450. [PubMed: 20022702]
4. Itoh M, Kiuru M, Cairo MS, Christiano AM. Proceedings of the National Academy of Sciences of the United States of America. 2011; 108:8797. [PubMed: 21555586]
5. Marino D, Luginbuhl J, Scola S, Meuli M, Reichmann E. Science translational medicine. 2014; 6:14.
6. Klar AS, Guven S, Biedermann T, Luginbuhl J, Bottcher-Haberzeth S, Meuli-Simmen C, Meuli M, Martin I, Scherberich A, Reichmann E. Biomaterials. 2014; 35:5065. [PubMed: 24680190]
7. Gibot L, Galbraith T, Huot J, Auger FA. Tissue engineering. Part A. 2010; 16:3199. [PubMed: 20528673]
8. Kim KL, Song SH, Choi KS, Suh W. Tissue engineering. Part A. 2013; 19:2478. [PubMed: 23790124]
9. Koffler J, Kaufman-Francis K, Shandalov Y, Egozi D, Pavlov DA, Landesberg A, Levenberg S. Proceedings of the National Academy of Sciences of the United States of America. 2011; 108:14789. [PubMed: 21878567]
10. Schechner JS, Nath AK, Zheng L, Kluger MS, Hughes CC, Sierra-Honigmann MR, Lorber MI, Tellides G, Kashgarian M, Bothwell AL, Pober JS. Proceedings of the National Academy of Sciences of the United States of America. 2000; 97:9191. [PubMed: 10890921]
11. Chen YC, Lin RZ, Qi H, Yang Y, Bae H, Melero-Martin JM, Khademhosseini A. Advanced functional materials. 2012; 22:2027. [PubMed: 22907987]
12. Miller JS, Stevens KR, Yang MT, Baker BM, Nguyen DH, Cohen DM, Toro E, Chen AA, Galie PA, Yu X, Chaturvedi R, Bhatia SN, Chen CS. Nature materials. 2012; 11:768. [PubMed: 22751181]
13. Gillette BM, Jensen JA, Tang B, Yang GJ, Bazargan-Lari A, Zhong M, Sia SK. Nature materials. 2008; 7:636. [PubMed: 18511938]
14. Wang XY, Jin ZH, Gan BW, Lv SW, Xie M, Huang WH. Lab on a chip. 2014; 14:2709. [PubMed: 24887141]
15. Moya ML, Hsu YH, Lee AP, Hughes CC, George SC. Tissue engineering. Part C, Methods. 2013; 19:730. [PubMed: 23320912]
16. Golden AP, Tien J. Lab on a chip. 2007; 7:720. [PubMed: 17538713]
17. Eastwood M, Porter R, Khan U, McGrouther G, Brown R. Journal of cellular physiology. 1996; 166:33. [PubMed: 8557773]
18. Gangatirkar P, Paquet-Fifield S, Li A, Rossi R, Kaur P. Nature protocols. 2007; 2:178. [PubMed: 17401352]
19. Abaci HE, Gledhill K, Guo Z, Christiano AM, Shuler ML. Lab on a chip. 2015; 15:882. [PubMed: 25490891]
20. Harrison CA, Gossiel F, Layton CM, Bullock AJ, Johnson T, Blumsohn A, MacNeil S. Tissue engineering. 2006; 12:3119. [PubMed: 17518627]
21. Braverman IM. The journal of investigative dermatology. Symposium proceedings / the Society for Investigative Dermatology, Inc. [and] European Society for Dermatological Research. 2000; 5:3.

22. Zheng Y, Chen J, Craven M, Choi NW, Totorica S, Diaz-Santana A, Kermani P, Hempstead B, Fischbach-Teschl C, Lopez JA, Stroock AD. Proceedings of the National Academy of Sciences of the United States of America. 2012; 109:9342. [PubMed: 22645376]
23. Zervantonakis IK, Hughes-Alford SK, Charest JL, Condeelis JS, Gertler FB, Kamm RD. Proceedings of the National Academy of Sciences of the United States of America. 2012; 109:13515. [PubMed: 22869695]
24. Corovic S, Markelc B, Dolinar M, Cemazar M, Jarm T. PloS one. 2015; 10:e0121370. [PubMed: 25793292]
25. Wu MH, Ustinova E, Granger HJ. The Journal of physiology. 2001; 532:785. [PubMed: 11313446]
26. Egawa G, Nakamizo S, Natsuaki Y, Doi H, Miyachi Y, Kabashima K. Scientific reports. 2013; 3:1932. [PubMed: 23732999]
27. Zhang Z, Michniak-Kohn BB. Pharmaceutics. 2012; 4:26. [PubMed: 24300178]
28. Chau DY, Johnson C, MacNeil S, Haycock JW, Ghaemmaghami AM. Biofabrication. 2013; 5:035011. [PubMed: 23880658]
29. Gledhill K, Guo Z, Umegaki-Arao N, Higgins CA, Itoh M, Christiano AM. PloS one. 2015; 10:e0136713. [PubMed: 26308443]
30. Huang S, Xu Y, Wu C, Sha D, Fu X. Biomaterials. 2010; 31:5520. [PubMed: 20398932]
31. Atac B, Wagner I, Horland R, Lauster R, Marx U, Tonevitsky AG, Azar RP, Lindner G. Lab on a chip. 2013; 13:3555. [PubMed: 23674126]
32. Varkey M, Ding J, Tredget EE. Tissue engineering. Part A. 2014; 20:716. [PubMed: 24090416]
33. Rhee S. Experimental & molecular medicine. 2009; 41:858. [PubMed: 19745603]
34. Taylor AM, Blurton-Jones M, Rhee SW, Cribbs DH, Cotman CW, Jeon NL. Nature methods. 2005; 2:599. [PubMed: 16094385]
35. Umegaki-Arao N, Pasmooij AM, Itoh M, Cerise JE, Guo Z, Levy B, Gostynski A, Rothman LR, Jonkman MF, Christiano AM. Sci Transl Med. 2014; 6:264ra164.
36. Itoh M, Umegaki-Arao N, Guo Z, Liu L, Higgins CA, Christiano AM. PLoS One. 2013; 8:e77673. [PubMed: 24147053]
37. Boyce ST, Kagan RJ, Greenhalgh DG, Warner P, Yakuboff KP, Palmieri T, Warden GD. The Journal of trauma. 2006; 60:821. [PubMed: 16612303]
38. Okita K, Matsumura Y, Sato Y, Okada A, Morizane A, Okamoto S, Hong H, Nakagawa M, Tanabe K, Tezuka K, Shibata T, Kunisada T, Takahashi M, Takahashi J, Saji H, Yamanaka S. Nature methods. 2011; 8:409. [PubMed: 21460823]
39. Okita K, Yamakawa T, Matsumura Y, Sato Y, Amano N, Watanabe A, Goshima N, Yamanaka S. Stem cells. 2013; 31:458. [PubMed: 23193063]
40. Lian X, Bao X, Al-Ahmad A, Liu J, Wu Y, Dong W, Dunn KK, Shusta EV, Palecek SP. Stem cell reports. 2014; 3:804. [PubMed: 25418725]
41. Carpenter AE, Jones TR, Lamprecht MR, Clarke C, Kang IH, Friman O, Guertin DA, Chang JH, Lindquist RA, Moffat J, Golland P, Sabatini DM. Genome biology. 2006; 7:R100. [PubMed: 17076895]
42. Garcia M, Escamez MJ, Carretero M, Mirones I, Martinez-Santamaria L, Navarro M, Jorcano JL, Meana A, Del Rio M, Larcher F. Molecular carcinogenesis. 2007; 46:741. [PubMed: 17610222]

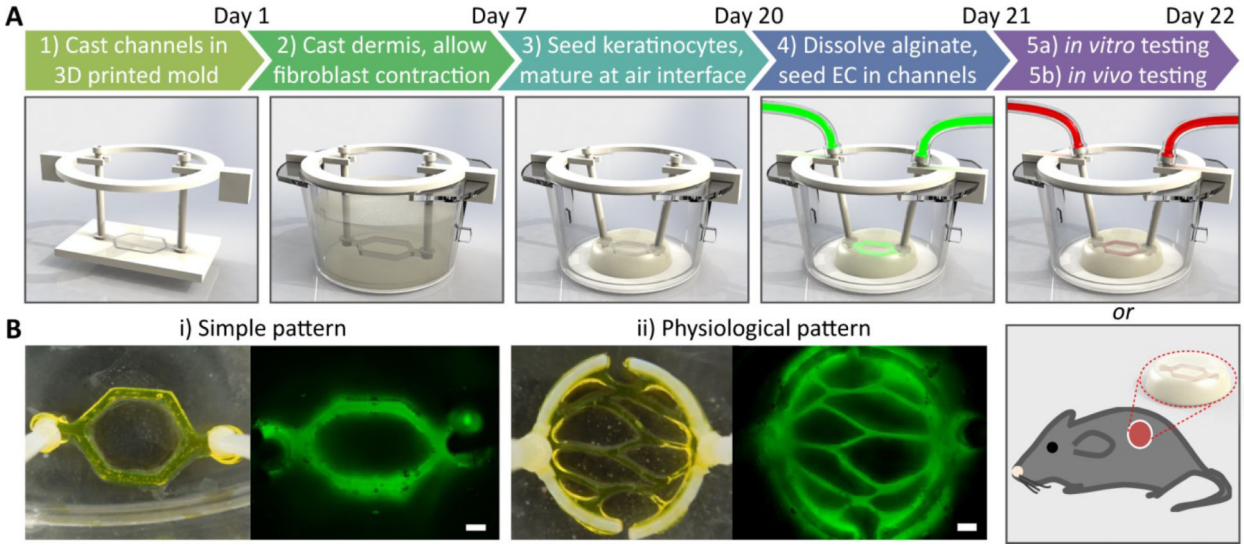

Figure 1. Development of vascularized HSEs

A) Schematic description of the protocol to develop vHSEs. Briefly, a sacrificial layer of alginate microchannels was created in 3D-printed molds, which had the desired vasculature pattern. Then the dermal compartment that consisted of dermal fibroblasts and collagen gel was formed around the sacrificial layer, which was suspended in the transwell inserts using a ring-shaped holder. After seeding the keratinocytes over the dermal compartment, the construct underwent epidermilization and cornification accompanied with a significant contraction. The sacrificial layer was dissolved by sodium citrate treatment through the inlet/outlet ports followed by EC seeding through the same ports. The vHSEs were then used either for grafting or in vitro perfusion experiments. **B)** Two different vasculature patterns were used in our studies and generated using fluorescently-tagged alginate. Scale bar: 600 μm.

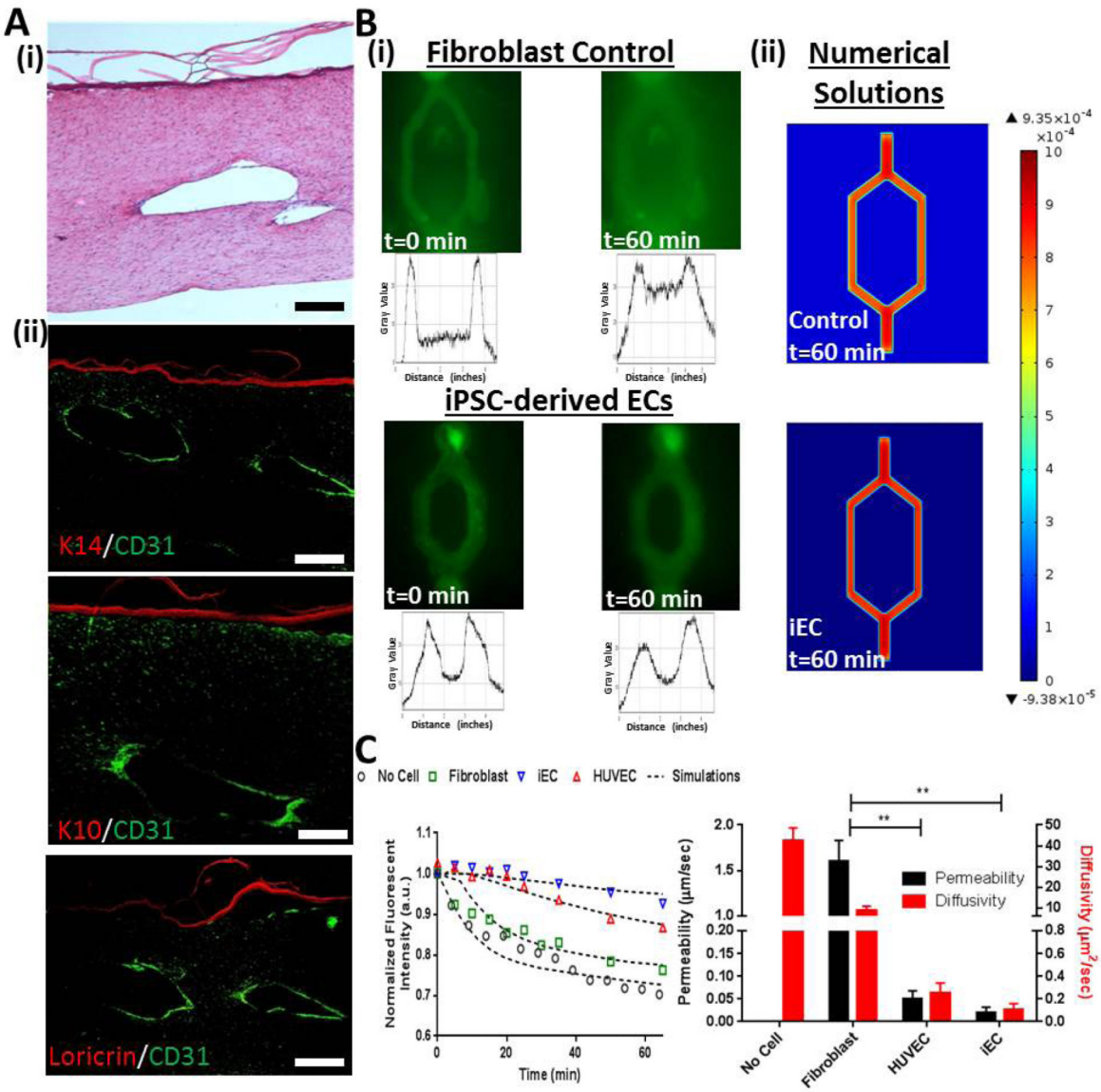

Figure 2. Epidermal integrity and endothelial barrier function in vHSEs

A) (i) H&E and **(ii)** immunofluorescent staining of histological sections of vHSE generated using iPSC-derived ECs. The sections were immunolabeled with K10, K14 and loricirin (red) and CD31 (green) to evaluate epidermal integrity and endothelial coating in the microchannels. Scale bars: 250 μm. **B)** Evaluation of the endothelial barrier function in vHSEs. **(i)** The microchannels seeded with fibroblasts or iPSC-derived ECs were perfused with a fluorescently tagged dextran (70 kDa) solution. Diffusion of the dye into the collagen gel was imaged for 60 mins and fluorescence intensity was quantified at each pixel along the horizontal centerline of images using ImageJ software. **(ii)** Distribution of the dextran in vHSEs after 60 mins was estimated using COMSOL Multiphysics software and represented in color surface plots for the microchannels with fibroblasts and iECs. The color spectrum depicts the dextran concentration ranging from dark red (highest) to dark blue (lowest). **C)** Quantification of the fluorescence intensity in the microchannels and estimated values of

permeability and diffusivity of the microchannels with fibroblasts, HUVECs, iECs or without cells. (**p<0.005 and N=3 HSEs)

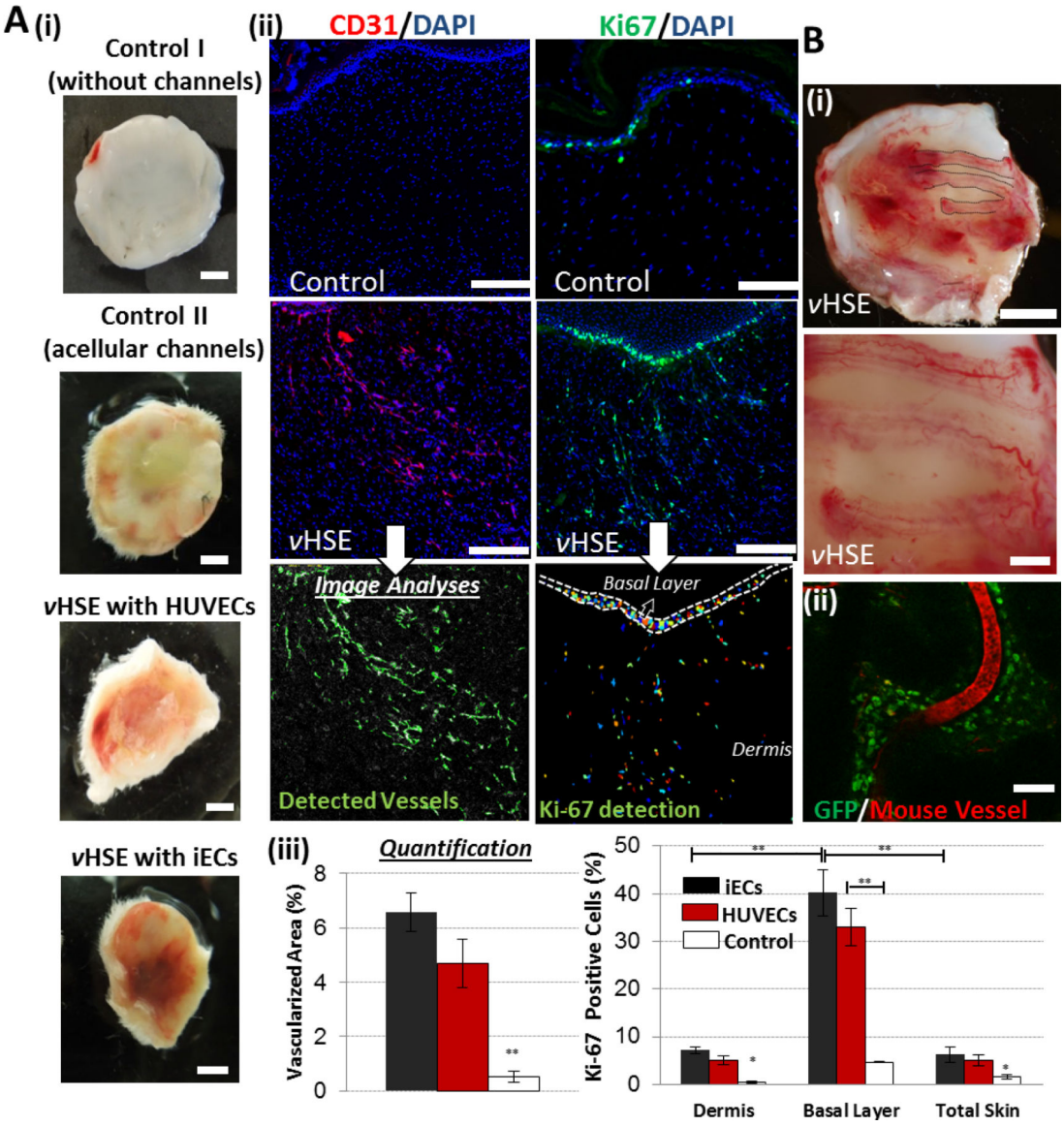

Figure 3. Engraftment of vHSEs onto SCID mice

A) The effect of vHSEs on host neovascularization. Blood perfusion in HSEs **(i)** without channels (Control I), with acellular microchannels (Control II), vHSEs with HUVECs, and iECs grafted on SCID mice and harvested after 2 weeks. Scale bar: 2.5 mm. **ii)** Immunostaining of explanted HSEs (control) and vHSEs with CD31 (red) and Ki67 (green) to visualize the invasion of the host vessels and the presence of proliferating cells, respectively. Scale bars: 250 μm. **iii)** Quantification of the percentage of the total area covered by the host vasculature and the percentage of Ki-67 positive cells (*$p<0.05$, **$p<0.005$ and N=4). **B)** The effect of vasculature pattern on the host neovascularization. **i)** Pictures of newly formed host vasculature following the micropatterned human iEC-containing microchannels in vHSEs in comparison to the HSEs containing microchannels with no cells. Scale bars: 2.5 mm and 500 μm **ii)** Confocal image of the explanted vHSEs showing the overlapping pattern of Rhodamine-dextran (70kDa) perfused mice vessels and

the microchannels containing GFP-tagged HUVECs. (N=4 for all conditions) Scale bar: 500 μm.